John von Neumann Institute for Computing



Conductance in Coupled Quantum Dots: Indicator for a Local Quantum Phase Transition

Frithjof B. Anders, Eran Lebanon, and Avraham Schiller

published in

NIC Symposium 2006 ,
G. Münster, D. Wolf, M. Kremer (Editors),
John von Neumann Institute for Computing, Jülich,
NIC Series, Vol. **32**, ISBN 3-00-017351-X, pp. 191-200, 2006.

© 2006 by John von Neumann Institute for Computing
Permission to make digital or hard copies of portions of this work for personal or classroom use is granted provided that the copies are not made or distributed for profit or commercial advantage and that copies bear this notice and the full citation on the first page. To copy otherwise requires prior specific permission by the publisher mentioned above.

http://www.fz-juelich.de/nic-series/volume32

Conductance in Coupled Quantum Dots: Indicator for a Local Quantum Phase Transition

Frithjof B. Anders[1,2], **Eran Lebanon**[3], **and Avraham Schiller**[4]

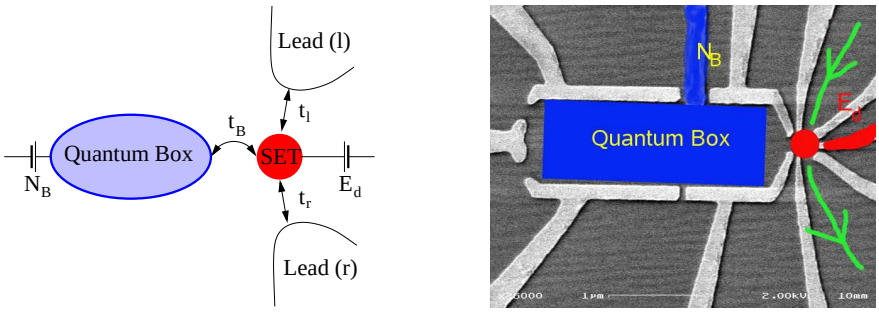
[1] Theoretische Physik, Universität des Saarlands
66041 Saarbrücken, Germany
[2] Institut für Theoretische Physik, Universtät Bremen
P.O. Box 330 440, 28334 Bremen, Germany *E-mail: anders@itp.uni-bremen.de*
[3] Department of Physics and Astronomy, Rutgers University
136 Frelinghuysen Road, Piscataway, NJ 08854-8019, USA
[4] Racah Institute of Physics, The Hebrew University
Jerusalem 91904, Israel

We report on transport properties of a nanostructed device consisting of an ultra-small quantum dot coupled to two leads and a larger quantum dot. The finite capacitance of both quantum dots leads to new and unusual transport properties when the temperature is lower than the charging energy E_c of the larger dot. The zero-bias transport is governed by the filling of the large dot as well as the ratio of the tunnel matrix elements between the small dot and leads, t_L, and between small and the large dot, t_B. For given external gate voltages of small and large dot, we find a critical ratio $t_c = t_B/t_L$ at which the zero-bias jumps from a high to a low conductance value. The quantum critical point is described by an unstable fixed point with non-Fermi liquid properties and governs the transition from one Fermi-liquid to another.

1 Introduction

Since the discovery of the Kondo effect in ultra-small quantum dots[1,2], nano-devices have become an increasingly important tool to test our fundamental understanding of elementary excitations in solid state physics. Measurements on the metallic heavy fermion (HF) compounds and high temperature superconductors[3,4] have challenged the paradigm of Landau's Fermi-liquid concept. For those deviations, the phenomenological term non-Fermi liquid (nFL) was attributed to such regimes appearing in a large variety of different materials[3,4]. The understanding of the observed nFL behavior is one of the most challenging and unsolved theoretical puzzles. In many materials, it is ascribed to a quantum critical point (QCP) at which a transition temperature is suppressed to $T = 0$ by an external control parameter such as pressure or doping[5,6].

Quantum dots behave in many respects as an artificial atom. One has experimental control over the "atomic" level position as well as coupling to the environment by external gate electrodes. Therefore, they are expected to be an ideal test system for concepts of *local quantum phase transitions*. In this work, we present numerical calculations on a system of coupled quantum dots as depicted in figure 1. Such a coupled quantum dot device consisting of a large quantum dot or quantum box and a small quantum dot or single electron transistor[7] (SET) undergoes a quantum phase transition at $T = 0$ for odd filling of the small dot which can be seen by the following arguments. When the small dot is tuned to odd occupation the $T \to 0$ physics is described by a strong coupling fixed point. If t_B is set to zero the dot is strongly coupled to the leads, and the conductance approaches its optimal (unitary) value. If, on the other hand, t_B finite and $t_l = t_r = 0$, the dot is coupled



(a) (b)

Figure 1. A sketch (a) of an ultra-small quantum dot coupled to two leads and a large quantum dot and its experimental realization by the group of D. Goldhaber-Gordon, who provided us with a picture of their realization.

strongly to the box (the renormalization group flow stops when T is reduced below the mean level spacing of the large dot), and the conductance is obviously zero. Switching on a very small coupling between the leads and the small dot does not change the physics since (i) the fixed point is stable, and (ii) the charging energy of the large dot will suppress charge fluctuations between leads and the small dot. Since these two limits are described by *two* complementary stable Fermi-liquid fixed points, there will be a quantum phase transition (QPT) at some critical coupling ratio $t_c = t_B/t_L$. This quantum critical point is associated with an unstable two-channel Kondo fixed point which has non-Fermi liquid properties[8]. Oreg and Goldhaber-Gordon conjectured the existence of such a non-Fermi liquid fixed point[9] for the local moment regime of the SET. We, however, have shown that the QPT is generic and associated with a dynamical generation of the channel symmetry and spin-conserving tunneling[10].

2 Modelling the Coulomb Blockade on Quantum Dots

Due to the confinement of the electrons in such an ultra-small quantum dot to a diameter of a few $100nm$, it has a mean one-particle level spacing of $\Delta E \approx 300 - 400\mu eV$ and a charging energy of $E_c \approx 1meV$. The energy on the dot is given by the Hamiltonian $\hat{H}_{qdot}$

$$\hat{H}_{qdot} = \sum_{i\sigma} E_i d^\dagger_{i\sigma} d_{i\sigma} + E_c \left(\hat{N} - N_B\right)^2 \tag{1}$$

where the charging energy $E_c = e^2/2C_0$ is related to the classical capacitance C_0 of the dot[7], and $\hat{N}$ measures its total number of electrons. Here, $d^\dagger_{i\sigma}$ creates an electron on the dot in level i with energy E_i and N_B denotes the external dimensionless potential governing the filling of the dot. Since spin-orbit scattering is proportional to the velocity it is strongly suppressed in quantum dots due to the confinement, and the pseudo spin σ is a good quantum number. The Hamiltonian (1) describes a classical capacitor for temperatures $k_B T \gg E_c$ with a linear dependence of the charge $Q = e\langle\hat{N}\rangle$ on the external voltage V. At temperatures much smaller that E_c, the quantization of the charge leads to

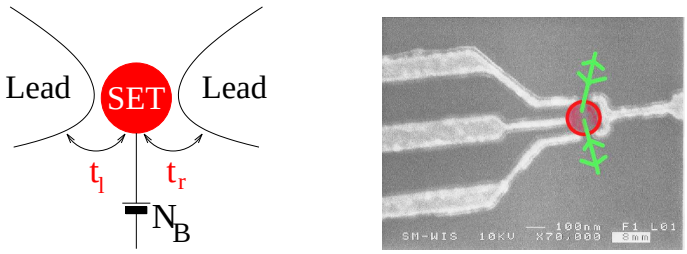


Figure 2. Single electron transistor[7] coupled to two leads (a) and its experimental realization, Figure taken from Ref.[1]

the discrete fillings. When $N_B = n + 1/2$, the energy is degenerate for the filling with n and $n + 1$ electrons. At $T = 0$, the charging will occur in steps as a function of N_B, and the charge Q is constant for $n - 1/2 < N_B < n + 1/2$.

2.1 Coupling to Leads

When coupling such a device weakly to two leads, as depicted in Fig. 2, a current can only flow at those charge degeneracy points for very small bias difference $|V_{sd}| \ll E_c$ and $k_B T \ll E_c$. Due to the finite charging energy, one electron can hop onto the dot only after the previous one has left the device, and the current flow is controllable by the potential N_B. The device operates as *single-electron transistor*[7] (SET) at temperatures $k_B T \ll E_c$. Characteristic for such a device are the nearly equally spaced conductance peaks as function of N_B from which E_c is obtained[7]. The width of these conductance peaks are fully determined by the temperature broadening which is used in commercially available low temperature thermometers[11].

If operated in a strong coupling mode, the line width is determined by the charge fluctuation scale $\Gamma_0 = \pi t^2 \rho_F$ rather than the temperature, where ρ_F denotes the density of states of the lead electrons at the chemical potential. At odd fillings, a new exponentially small low energy scale $T_K \propto \exp(-\alpha E_c/\Gamma_0)$ occurs due to the Kondo effect[12] (α measures the particle-hole asymmetry.) At temperatures below this crossover scale T_K an additional conduction channel opens up, and the Coulomb blockade is lifted[1]. Therefore, an increasing conductance is experimentally observed for decreasing T[1,2] saturating at the unitary limit of $2e^2/h$. In order to observe the Kondo effect experimentally, the devices are operated in a strong coupling regime of $k_B T \ll \Gamma \approx E_c/10$.

For ultra-small quantum dots, ΔE is larger than the charge fluctuation scale, $\Delta E > \Gamma_0$. At sufficiently low temperatures ($\beta \Delta E > 1$,) $\hat{H}_{qdot}$ can be replaced by an single effective spin degenerate level with the external controllable energy $E_d \propto N_B$ and the Coulomb repulsion U. In this case, Eqn. (2) is identical to the single impurity Anderson model[13].

2.2 Description of the Coulomb Blockade of a Large Quantum Dot

The coupled quantum dot–lead system is conventionally modelled by the Hamiltonian

$$\mathcal{H} = \hat{H}_{qdot} + \sum_{\gamma=l,r} \sum_{k\sigma} \epsilon_{\gamma k} c^\dagger_{\gamma k\sigma} c_{\gamma k\sigma} + \sum_\gamma t_\gamma \sum_{k,i\sigma} \left(c^\dagger_{\gamma k\sigma} c_{i\sigma} + \text{H.c.} \right), \tag{2}$$

where $c^\dagger_{\gamma k\sigma}$ creates a lead electron with momentum k and spin σ in the lead $\gamma = l, r$. t_γ is the tunneling matrix element, taken for simplicity to be momentum and level independent. The single-particle levels in the leads $\epsilon_{\gamma k}$ are assumed to be continuous (dense energy levels). It is obvious, that in equilibrium only the binding linear combination of lead states $c_{k\sigma} = (t_l c_{Lk\sigma} + t_r c_{Rk\sigma})/\sqrt{t_l^2 + t_r^2}$ couples to the quantum dot with the effective tunnel matrix element $t_L = \sqrt{t_l^2 + t_r^2}$. We drop the anti-binding combination and treat the leads as as single fermionic bath.

Since the charging term $E_c(\hat{N} - N_B)^2$ in $\hat{H}_{qdot}$ is long ranged for a large dot with many one-particle levels, perturbation theory as well as RG methods fail to describe the crossover from the classical to the quantum regime of Hamiltonian (2). The problem becomes accessible to Wilson's numerical renormalization group (NRG) by introducing an effective charge degree of freedom $\hat{N} = \sum_n n|n\rangle\langle n|$ and the corresponding ladder operators $N^\pm = \sum_n |n \pm 1\rangle\langle n|$ independent of the number of Fermions. The price is a modification of the tunneling term[14] to

$$H_T = t \sum_{ik\sigma} \left(c^\dagger_{k\sigma} c_{i\sigma} N^- + c^\dagger_{i\sigma} c_{k\sigma} N^+ \right) \tag{3}$$

in order to keep track of the change of charge on the dot. The charging term $E_c(\hat{N} - N_B)^2$ becomes part of an effective impurity, and H_T can easily be treated within the NRG. We have shown that our theory describes accurately the crossover from the classical to the quantum regime[14] for all parameter regimes. Moreover, the effective capacitance diverges logarithmically with temperature at the charge step, indicating a quantum phase transition between two Fermi-liquids with different dot charges. The QCP is characterized by a charge two channel Kondo fixed point[14,15].

3 Modelling of Coupled Quantum Dots

Interesting new physics[9,10,16] arises when we combine these two limits for quantum-dots into one single nano-device. An ultra-small quantum dot with a large level spacing is coupled to two leads and also to a quantum box. This device and its experimental realization is shown in Fig. 1. For $k_B T \gg E_c$, the device behaves as simple SET. For $\beta E_c \gg E_c$, however, a second conduction channel is dynamically generated: charge fluctuations from the leads to the quantum box through the SET, possible at high temperatures, are now suppressed. We expect a quantum phase transition as function of the ratio t_B/t_L where the quantum critical point is described by a non-Fermi liquid fixed point.

The Hamiltonian for such a device is given by extension[10] of (2)

$$\begin{aligned} \mathcal{H} = &\sum_\sigma (E_d + \frac{U}{2} n_{-\sigma}) n_\sigma + E_c(\hat{N} - N_B)^2 + \sum_{\alpha=L,B,k\sigma} \epsilon_{\alpha k} c^\dagger_{\alpha k\sigma} c_{\alpha k\sigma} \\ &+ t_L \sum_{k\sigma} \left(c^\dagger_{Lk\sigma} d_\sigma + d^\dagger_\sigma c_{Lk\sigma} \right) + t_B \sum_{k\sigma} \left(c^\dagger_{Bk\sigma} d_\sigma N^+ + d^\dagger_\sigma c_{Bk\sigma} N^- \right), \end{aligned} \tag{4}$$

where we restrict ourselves to a single level with energy E_d on the SET and to the binding combination of lead states. The charging energy of the SET is given by U. While electrons tunnel between the binding combination of leads and SET with the amplitude t_L, the tunneling term to the quantum box is modified by the ladder operators $N^{\pm}$ in order to take into account the change of charge.

4 Theory

We accurately solve Hamiltonian (4) using Wilson's numerical renormalization group[12,17] best suited for this quantum impurity problem. The key ingredient in the NRG is a logarithmic discretization of the continuous bath, controlled by the parameter $\Lambda > 1$[12]. The Hamiltonian is mapped onto a semi-infinite chain, where the Nth link represents an exponentially decreasing energy scale $D_N \sim \Lambda^{-N/2}$. Using this hierarchy of scales the sequence of finite-size Hamiltonians $\mathcal{H}_N$ for the N-site chain is solved iteratively, truncating the high-energy states at the conclusion of each step so as to maintain a manageable number of states. The reduced basis set of $\mathcal{H}_N$ so obtained faithfully describes the spectrum of the full Hamiltonian on a scale of D_N, corresponding to the temperature $T_N \sim {D_N}$[12] from which all thermodynamic expectation values are calculated.

In addition to the total spin component S_z^{tot}, we also use the particle number and the conserved flavor $\tau_z^{tot} = \hat{N} + (\hat{N}_L - \hat{N}_B)/2$ to classify the symmetries of subspaces of the Hamiltonians H_N. Since all subspaces can be diagonalized independently, we have fully parallelized our NRG code on the IBM Regatta using POSIX threads. The setup of the Hamiltonian matrices is mainly performed using ESSL and BLAS routines so that our C^{++} code runs highly efficiently on SMP platforms such as the Regatta.

5 Results

5.1 Thermodynamics

By investigating the effective capacitance of the quantum box, $C_{eff} = e\partial\langle N\rangle/\partial N_B$ near the charge step[16], we have shown that $C_{eff}(T)$ diverges logarithmically for a particular gate voltage at fixed coupling ratio: the slope of the charge becomes infinitely steep. The associated non-Fermi liquid quantum critical point consists of a charge two-channel Kondo fixed point[15,8] plus a marginal operator describing the particle-hole asymmetry[18]. The charge on the quantum box is screened through charge fluctuations[16] with the SET which resembles an anisotropic Kondo interaction in the flavor space[15].

In this work, we focus on the local spin screening. For a given set of parameters, we tune the ratio t_B/t_L to its critical value t_c such that the Pauli-like local spin susceptibility of the SET $\chi_{spin} = \partial\langle\hat{S}_z^{SET}\rangle/\partial_H$, for $|t_B/t_L - t_c| > 0$ becomes logarithmically divergent at t_c. The results of such computational expensive scans are depicted in Fig. 3 for different values of gate voltage E_d of the SET and experimentally typical ratios of parameters $U/E_c \approx 10$, $E_c/\Gamma_L = 1$. By fitting of χ to $\chi(T) = -(1/20T_K^{QPT})\ln\left(T/T_K^{QPT}\right) + b$, we have extracted the characteristic energy scale T_K^{QPT} of the non-Fermi liquid fixed point. The crossover from a Curie law to a logarithmically divergent $\chi(T)$ approaching the QCP is governed by $T_{min} = \min\{T_K, E_c\}$. We observed that the charge[16] and spin[9,10] QCP

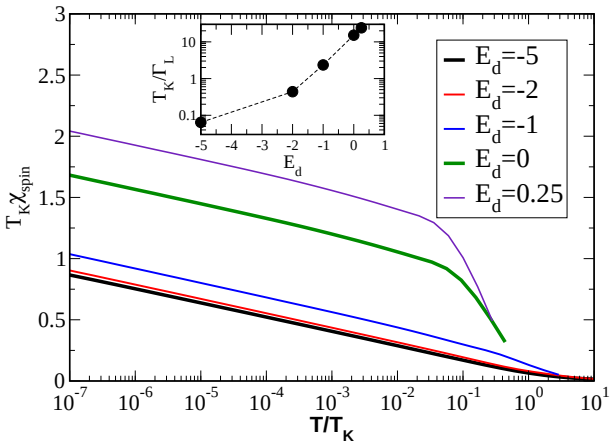


Figure 3. The spin susceptibility χ of the dot versus T, for $\Gamma_L = E_c = 0.1D$, $N_B = 0$, $U/E_c = 10$ and different gate voltages E_d. Here t_B is tuned for each value of U to quantum phase transition. Inset: T_K versus E_d. NRG parameters: $\Lambda = 2.8$, $N_s = 2000$.

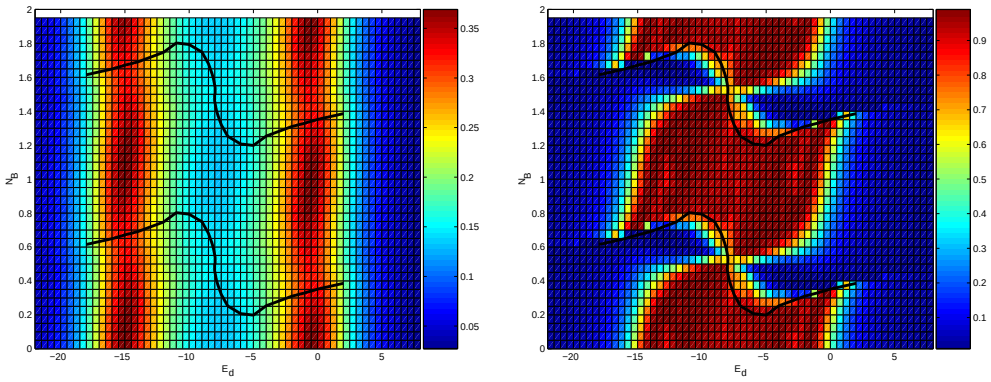


Figure 4. Color coded zero Bias conductance as function of the two gate voltages E_d and N_B for a fixed coupling ratio $t_B^2/t_L^2 = 1.2$ and $E_c/\Gamma_L = 2, U/\Gamma = 16$ at (a) $T/\Gamma_L = 0.65$. and (b) $T/\Gamma_L = 3.1 * 10^{-4}$. The black line indicates the quantum critical line. NRG parameters: $\Lambda = 4$, $N_s = 800$. Each point consumed about 15h CPU time on the IBM Regatta.

points are connected, in fact, can be identical. That implies that this distinction is somewhat misleading and arises since physical operators such as charge, spin or flavor (not investigated yet) couple with different matrix elements to the leading irrelevant operator of the non-Fermi liquid fixed point.

5.2 Zero-Bias Conductance

For calculating the zero bias conductance $G(T)$ through the SET,

$$G(T)/G_0 = \Gamma_L \sum_\sigma \int d\omega \, \left(-\frac{\partial f(\omega)}{\partial \omega}\right) \rho_\sigma^d(\omega, T) \tag{5}$$

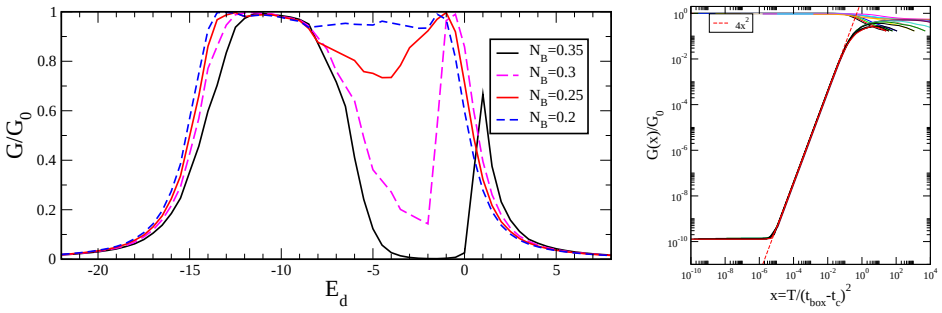
we need the finite temperature spectral function $\rho_\sigma^d(\omega)$ of the Green function $\ll d_\sigma | d_\sigma^\dagger \gg$, where $\Gamma_L = \pi t_L^2 \rho_F$, and $G_0 = (2e^2/h) 4 t_l^2 t_r^2/(t_r^2 + t_r^2)^2$ measures the optimal conductance for generic couplings t_l and t_r between the two leads where $t_L^2 = t_l^2 + t_r^2$. The spectral function obtained directly with the NRG, however, is not accurate enough to calculate the conductance reliably. We use an equation of motion[19,20] technique in combination with an new algorithm to calculate finite temperature spectral functions for multi-band models as described in detail in the appendix of reference[21]. Since our algorithm allows to evaluate $\rho(\omega, T)$ independently for each ω, we use a massively parallelized algorithm to generate $\rho(\omega, T)$ for frequencies on a logarithmic mesh for a whole set of frequencies and temperatures independently in one NRG run.

Experimentally, however, the ratio of t_B/t_L is kept fixed since t_α does not depend linearly on the external potentials. The zero bias conductance for large set of parameters (E_d, N_B) at fixed $t_B^2/t_L^2 = 1.2$ is plotted for two different temperatures in Fig. 4. Since each color point stems from one NRG run, we needed to reduce the number of state N_s kept at each iteration and increase Λ. At high temperatures, $k_B T \approx E_c/4$, the conductance is almost independent of the filling of the large dot. The conductance peaks at the charge steps of the small dot at $E_d/\Gamma_L \approx -15$ and $E_d \approx 0$. The picture changes completely at low temperatures. For $N_B \approx 0$, we find a regime of high conductance at filling $\langle n_d \rangle \approx 1$ due to the Kondo effect where the conductance is close to the optimal conductance G_0. At an E_d dependent value of N_B, however, we observe sharp drop in the conductance. This correlates with the quantum critical line (QCL) added as a black line in the plots. On the other hand, the conductance changes gradually at half integer filling of the coupled dot which occurs at $-15 < E_d < -12$ in the depicted conductance plots of Fig. 5.

The conductance for four different values of N_B, horizontal lines in Fig. 4b, is depicted in 5a. For $N_B = 0.2$, the QCL is not crossed and the usual lifting of the Coulomb blockade due to the Kondo effect is seen at odd SET filling between $-16 < E_d < 0$. For $N_B = 0.25, 0.3, 0.35$, the parameter E_d intersects twice the QCL as can be seen in Fig.4. Consequently, the three curves for $N_B = 0.25, 0.3, 0.35$ show a pronounced supression of the conductance between these intersection points. At $T = 0$, the conductance will exhibit a jump at these two intersection values of E_d defining the QCP. For particle-hole symmetry, the conductance curves collapse onto two master curves when scaled as $x = T/(t_B/t_L - t_c)^2$ shown in Fig. 5b.

6 Concluding Remarks

We calculate the thermodynamical and transport properties of a novel coupled quantum dot device using our extension to the NRG. Since the subspaces of the Hamiltonians can be diagonalized independently, we can use a highly efficient parallelized code on the IBM Regatta to solve this complex many-body problem accurately. We find a line of quantum critical points which governs the crossover from a high to a low conducting Fermi liquid.



(a) (b)

Figure 5. Conductance (a) vs E_d for four different values of N_B at $T/\Gamma_L = 3.1 * 10^{-4}$. For $N_B = 0.2$, the Coulomb blockade is lifted, and $G/G_0 \approx 1$ for $\langle n_d \rangle \approx 1$. For $N_B > 0.2$ the QCL is crossed twice leading to sudden decrease of G. Data taken from Fig. 4. (b) Conductance vs $x = T/(t_B/t_L - t_c)^2$ (b) for $E_d/\Gamma_0 = -5$, $U/\Gamma_0 = 10$, $N_B = 0$, $\Lambda = 2.8$ and $N_s = 2500$ and 21 different values of t_B/t_L.

We showed that the zero-bias conductance can be used to indicate the phase line since a drop of the conductance is observed which becomes increasingly sharp. Since our theory is valid for arbitrary parameters, we can make contact to the experimentally relevant parameter regime where spin and charge fluctuation scales are not well separated.

Acknowledgments

We have benefited from discussions with D. Goldhaber-Gordon and R. Potok and are thankful for letting us use the image of their device. F.B.A. acknowledges funding of the NIC, Forschungszentrum Jülich, under project no. HHB000. EL was supported by DOE grant DEFE02-00ER45790.

References

1. D. Goldhaber-Gordon *et al.*, Nature **391**, 156 (1998).
2. W.G. van der Wiel *et al.*, Science **289**, 2105 (2000).
3. M. B. Maple *et al.*, J. Low Temp. Phys. **99**, 223 (1995).
4. G. R. Stewart, Rev. Mod. Phys **73**, 797 (2001).
5. H. von Löhneyen, J. Phys., Condens. Matter **8**, 9689 (1996).
6. F. Steglich *et al.*, J. Phys., Condens. Matter **8**, 9909 (1996).
7. M A Kastner, Rev. Mod. Phys. **64**, 849 (1992).
8. D. L. Cox and A. Zawadowski, Advances in Physics **47**, 599 (1998).
9. Y. Oreg and D. Goldhaber-Gordon, Phys. Rev. Lett. **90**, 136602 (2003).
10. F. B. Anders, E. Lebanon, and A. Schiller, Phys. Rev. B **70**, 201306 (2004).
11. J. P. Pekola *et al.*, Phys. Rev. Lett. **73**, 2903 (1994).
12. K. G. Wilson, Rev. Mod. Phys. **47**, 773 (175).
13. P. W. Anderson, Phys. Rev. **124**, 41 (1961).
14. E Lebanon, A Schiller, and F B Anders, Phys. Rev. B **68**, 041311 (2003).

15. K A Matveev, Zh. Eksp. Teor. Fiz. **99**, 1598 (1991).
16. E. Lebanon, A. Schiller, and F. B. Anders, Phys. Rev. B **68**, 155301 (2003).
17. H. R. Krishna-murthy, J. W. Wilkins, and K. G. Wilson, Phys. Rev. B **21**, 1003 (1980).
18. H. R. Krishna-murthy, J. W. Wilkins, and K. G. Wilson, Phys. Rev. B **21**, 1044 (1980).
19. R. Bulla, A. C. Hewson, and Th. Pruschke, J. Phys., Condens. Matter **10**, 8365 (1998).
20. F. B. Anders, Phys. Rev. B **71**, 121101 (2005).
21. F. B. Anders and G. Czycholl, Phys. Rev. B **71**, 125101 (2005).